Dalton
Transactions

ROYAL SOCIETY
OF CHEMISTRY

PAPER
Beata Nowicka and Michał Heczko
Switching of magnetic properties by topotactic reaction in a
1D CN-bridged Ni(II)–Nb(IV) system

Check for updates

Switching of magnetic properties by topotactic reaction in a 1D CN-bridged Ni(II)−Nb(IV) system†

Michał Heczko (ID) and Beata Nowicka (ID) *

Two 1D CN-bridged assemblies: the nearly straight $Li_2[Ni(cyclam)][Nb(CN)_8] \cdot 7.5H_2O$ (**1**) chains and the zigzag-shaped $Li_2[Ni(cyclam)][Nb(CN)_8] \cdot 2H_2O$ (**2**) chains, are obtained in the reaction between [Ni (cyclam)]$^{2+}$ and [Nb(CN)$_8$]$^{4-}$ in warm concentrated LiCl water solution. Both compounds are composed of alternating bimetallic Ni(II)−Nb(IV) chains and contain incorporated lithium cations, which compensate the negative charge of the coordination skeleton. The straight chain **1** (Ni−Nb−Ni angle = 153.2°) can be reversibly dehydrated under dry nitrogen flow at room temperature to an intermediate dihydrate phase **1d** and further transformed to the zigzag-shaped chain **2** (Ni−Nb−Ni angle = 86.6°) by annealing at 150 °C. The process can be reversed by exposure to high humidity at room temperature, upon which **2** is converted back to **1**. This water sorption-induced breathing effect is accompanied by changes in magnetic properties, most notably reflected in different values of saturation magnetization and critical field of meta-magnetic transition, which indicate that both intra- and inter-chain interactions are affected by the structure reorganization.

Introduction

Cyano-bridged coordination polymers constitute an important group of molecular magnetic materials. The CN ligand mediates relatively strong magnetic interactions and simultaneously allows the formation of versatile structures of different topologies, incorporating organic parts, which may serve as platforms for the introduction of additional properties.[1–5] The flexibility of CN-bridged frameworks enables the design of non-rigid structures, in which magnetic properties can be modified by the inclusion of guest molecules or ions. Octacyanoniobate(IV) ion has shown great potential in the construction of multifunctional bimetallic assemblies.[6,7] The 3D Nb-based networks with high connectivity show relatively high magnetic ordering temperatures,[8,9] with the record value of T_C = 210 K among the octacyanometallate-based assemblies for the V$^{II/III}$–Nb^{IV} 3D network.[9] Some networks with additional organic ligands were found to undergo structural changes upon reversible dehydration, which enables post-synthetic modifications and tuning of T_C.[10,11] Several [Nb(CN)$_8$]$^{4-}$ – based compounds show marked magnetocaloric effect,[12] including very rare rotating magnetocaloric effect, connected with high magnetic anisotropy.[13,14] There are also examples of

chiral networks, which exhibit interesting magneto-optical cross effects, including magnetically enhanced second harmonic generation.[15] Notably, there is only one report on an octacyanidoniobate(IV)-based 1D coordination polymer.[16] It was obtained by the combination of [Nb(CN)$_8$]$^{4-}$ anions with Mn^{2+} cations coordinated by a flat pentadentate ligand and it shows the topology of a chain with pendant arms. More 1D assemblies are known for analogous tetravalent octacyanidometallates of group 6 metals. They show different topologies, including ladder,[17] vertex-sharing squares,[18,19] or vertex-sharing trigonal bipyramids.[20] However, since [M(CN)$_8$]$^{4-}$ (M = Mo^{IV}, W^{IV}) ions are diamagnetic, these chain structures do not show magnetic interactions through CN-bridges, which in many cases lead to interesting phenomena including single chain magnet behaviour.[21,22]

We have shown before the possibility of manipulating the dimensionality and topology of the CN-bridged assemblies based on [Ni(cyclam)]$^{2+}$ and tetravalent [M(CN)$_8$]$^{4-}$ ions (M = Mo^{IV}, W^{IV}) by the addition of LiCl and changing reaction conditions. For the W^{IV}-based precursor we have obtained as many as five coordination polymers of different topology and dimensionality, which include a 3D diamond-like network [Ni (cyclam)]$_2$[W(CN)$_8$] $\cdot$16H$_2$O, a microporous 2D honeycomb-like network incorporating Li$^+$ ions Li$_2$[Ni(cyclam)]$_3$[W (CN)$_8$]$_2 \cdot$24H$_2$O, a 3D two-fold interpenetrating network [Ni (cyclam)]$_5$[Ni(CN)$_4$][W(CN)$_8$]$_2 \cdot$11H$_2$O formed as a result of rearrangement of the building blocks, as well as 1D linear and zigzag-shaped chains.[23] Mo^{IV}-based analogues comprise 3D and 2D structures[24] and show interesting photomagnetic pro-

Faculty of Chemistry, Jagiellonian University, Gronostajowa 2, 30-387 Kraków, Poland. E-mail: beata.nowicka@uj.edu.pl

perties modified by water sorption.[23] By replacing the diamagnetic octacyanidometallates of Mo^{IV} and W^{IV} with paramagnetic $[Nb(CN)_8]^{4-}$ ions we have constructed a series of 2D honeycomb-like frameworks with tuneable magnetic properties by incorporation of different guest cations.[25,26] Here we present the first alternating bimetallic chain composed of octacyanidoniobate(IV) and Ni(II) ions, obtained by the synthetic strategy based on the addition of non-coordinating s-block cations at elevated temperature.[23]

Experimental section

Materials

The $[Ni(cyclam)(NO_3)_2]$ and $K_4[Nb(CN)_8]\cdot 2H_2O$ precursor complexes were synthesized according to literature methods.[27] The lithium chloride salt and all solvents were commercially available and used as supplied.

Synthesis of compounds

$Li_2[Ni(cyclam)][Nb(CN)_8]\cdot 7.5H_2O$ (1). A water solution (7 mL) containing $[Ni(cyclam)(NO_3)_2]$ (20 mg, 0.05 mmol) and lithium chloride (3 g, 71 mmol) was heated to the temperature of 50 °C. Then, the water solution (3 mL) of $K_4[Nb(CN)_8]\cdot 2H_2O$ (25 mg, 0.05 mmol) and LiCl (2 g, 47 mmol) was heated to the temperature of 35 °C. The solutions were mixed and slowly cooled to the temperature of about 30 °C. While the solution was getting cold the yellow plate-shaped crystals of **1** formed together with the needle-shaped crystals of **2**. The final mixture was sealed and kept in a water bath (35 °C) for a week, in which the needles of **2** recrystallized to well-formed plates of **1**. The final product was filtered off and washed with a small amount of cold THF and acetone and then dried in the air. Yield: 80%. Elemental analysis: found: C: 30.32, N: 23.60, H: 5.36% (C/N: 1.285); calculated for: $C_{18}H_{39}Li_2N_{12}NbNiO_{7.5}$: C: 30.49, N: 23.70, H: 5.54% (C/N: 1.287). $M = 709.06$ g mol^{-1}. IR $\nu(CN)$: 2124s, 2140s, 2145sh cm^{-1}.

$Li_2[Ni(cyclam)][Nb(CN)_8]\cdot 2H_2O$ (1d). The dehydrated phase of **1** was obtained by drying crystals in a vacuum (ca. 1 day) or under nitrogen gas flow. IR $\nu(CN)$: 2120s; 2135sh cm^{-1}.

$Li_2[Ni(cyclam)][Nb(CN)_8]\cdot 2H_2O$ (2). The yellow needle-shaped crystals of **2**, suitable for SC-XRD measurement, were obtained as a by-product in the synthesis of **1**. This compound could also be obtained in powder form by heating dry crystals of **1** at the temperature of 150 °C, which was additionally confirmed by PXRD. Elemental analysis: found: C: 34.45, N: 26.69, H: 4.82% (C/N: 1.290); calculated for: $C_{18}H_{30}Li_2N_{12}NbNiO_3$: C: 34.43, N: 26.76, H: 4.82% (C/N: 1.287). $M = 627.99$ g mol^{-1}. IR $\nu(CN)$: 2121sh; 2132s cm^{-1}.

Structure determination

The single crystal X-ray diffraction measurements for **1** and **2** were performed on a Bruker D8 Quest diffractometer equipped with a Mo Kα radiation source ($\lambda = 0.71073$ Å). The structures were solved by direct methods using SHELXT and the refinement was performed using SHELXL.[28] All the non-hydrogen

atoms were refined anisotropically. The C–H and N–H hydrogen atoms were placed in idealized positions and refined isotropically using the riding model with $U_{iso}(H)$ equal to $1.2U_{eq}$ for the C or N atoms. The H-atoms of crystallization water were found from the difference electron density map. Graphical representations of the structures were prepared with the Mercury CSD 4.3.1 software.[29] The analysis of the coordination polyhedra was performed using SHAPE 2.1.[30] The crystallographic data are presented in Table 1. CCDC deposition numbers: 2280169 (**1**), 2280170 (**2**).†

Physical measurements

Powder X-ray diffraction data were collected on a Bruker D8 Advance Eco diffractometer equipped with a Cu Kα radiation source ($\lambda = 1.541874$ Å), in the Debye–Scherrer geometry. The microcrystalline samples were sealed in glass capillaries and measured in the 5–50° 2θ range at room temperature. The reference powder patterns from SC-XRD measurements were generated using Mercury CSD 4.3.1 software.[29] Elemental analyses of CHN were performed on an ELEMENTAR Vario Micro Cube CHNS analyser. IR spectra were collected on a Bruker Alpha II spectrometer with a diamond ATR add-on. The thermogravimetric data were collected using a Netzsch TG 209 F1 Libra apparatus. The water sorption/desorption processes were characterized by the dynamic vapor sorption method using the SMS DVS Resolution apparatus. The isotherm was measured in a 0–90% relative humidity range at a temperature of 25 °C. Every measurement step was performed until a stable

Table 1 Crystallographic data for **1** and **2**

Compound	1	2
Empirical formula	$C_{18}H_{36}Li_2N_{12}NbNiO_6$	$C_{18}H_{28}Li_2N_{12}NbNiO_2$
FW	682.09	610.02
T (K)	100	100
Crystal system	Monoclinic	Monoclinic
Space group	$P2/n$	$C2/c$
a (Å)	10.2590(8)	12.2706(4)
b (Å)	9.6405(7)	14.4329(5)
c (Å)	15.8896(12)	14.6110(5)
α (°)	90	90
β (°)	105.385(2)	94.782(1)
γ (°)	90	90
V (Å^3)	1515.2(2)	2578.61(15)
Z	2	4
V/Z (Å^3)	757.6	644.7
$\rho_{calc.}$ (Mg m^{-3})	1.495	1.571
μ (mm^{-1})	1.051	1.214
$F(000)$	702	1244
Crystal size (mm)	0.17 × 0.07 × 0.03	0.40 × 0.04 × 0.03
θ range (°)	2.50–27.5	2.50–26.4
Reflections collected	21 012	15 907
Independent	3483	2641
Observed	3293	2455
Parameters	201	171
R_{int}	0.030	0.026
GOF on F^2	1.206	1.186
R_1 [$I > 2\sigma(I)$]	0.0293	0.0230
wR_2 (all data)	0.0579	0.0476
CCDC deposition number	2280169	2280170

mass was achieved. Magnetic susceptibility measurements were performed on a Quantum Design MPMS-3 Evercool magnetometer in magnetic fields up to 70 kOe. The experimental data were corrected for diamagnetism of the sample and the sample holder. The magnetic data were fitted using the PHI programme.[31]

Results and discussion

Synthesis strategy, materials stability, and sorption properties

The combination of the cationic $[Ni(cyclam)]^{2+}$ building block with polycyanometallate anions led to the formation of a wide group of CN-bridged coordination polymers characterized by diverse network dimensionality and topology.[23–26] Moreover, the final product characteristics often depended on the reaction conditions including type of solvent, temperature, presence of additional ions, and building block ratio. We have previously proved that it is possible to obtain as many as six various coordination systems based on $[Ni(cyclam)]^{2+}$ and $[W(CN)_8]^{4-}$ by the manipulation of the above factors.[23] The reaction between $[Ni(cyclam)]^{2+}$ and $[Nb(CN)_8]^{4-}$ performed in water solution leads to the formation of a neutral coordination network of the formula $[Ni(cyclam)]_2[Nb(CN)_8]\cdot nH_2O$,[32] which is the most thermodynamically stable phase. When the reaction is carried out in the presence of additional electrolytes at room temperature, the incorporation of appropriate cations into the coordination framework was observed. It resulted in the formation of two-dimensional networks, characterized by the honeycomb-like topology, of the general formula $M_x[Ni(cyclam)]_3[Nb(CN)_8]_2\cdot nH_2O$ (x = 2: M = Li^+, Na^+, NH_4^+; x = 1: M = Mg^{2+}, Ca^{2+}, Sr^{2+}, Ba^{2+}).[25,26] However, these compounds upon contact with water recrystallize to the neutral Ni_2Nb network.[32]

In order to construct a 1D $Ni^{II}-Nb^{IV}$ coordination polymer we used the slightly modified synthetic procedure by which an analogous linear $Ni^{II}-W^{IV}$ chain was obtained.[23] The reaction temperature was kept below 45 °C in order to avoid the decomposition of the $[Nb(CN)_8]^{4-}$ complex, which is less robust than $[W(CN)_8]^{4-}$. The 1420-fold excess of LiCl was used. When the warm solutions of the building blocks were combined and allowed to cool, two types of crystals were formed: plates of the $Li_2[Ni(cyclam)][Nb(CN)_8]\cdot7.5H_2O$ straight chain (**1**) and needles of the $Li_2[Ni(cyclam)][Nb(CN)_8]\cdot2H_2O$ zigzag chain (**2**). If the reaction mixture was kept at 35 °C for a week the needle-shaped crystals of **2** recrystallized into well-formed plate-shaped crystals of **1**. The purity of the final product was confirmed by powder X-ray diffraction measurement on the sample in mother liquor (Fig. S1†). The recrystallization process suggests that **1** is the thermodynamically favoured phase. The crystals of **1** are stable under mother liquor and in concentrated lithium chloride solution. Upon even short contact with water, the crystals collapse into a fine powder and the compound decomposes. Therefore, in order to remove the remains of highly hygroscopic LiCl, after filtration the crystals of **1** were washed with a small amount of cold (4 °C) tetrahydrofuran, in which LiCl is soluble, and then with cold

acetone. The crystals of **1** treated that way are stable under ambient temperature and humidity conditions, as shown by PXRD (Fig. S1†).

The water sorption/desorption measurements, performed using the dynamic vapor sorption gravimetric method (DVS), indicate that the fully hydrated phase containing $7.5H_2O$ per formula unit is stable in the range of 90–2% RH (Fig. 1). Dehydration takes place under dry nitrogen flow at room temperature which leads to phase **1d** containing $2H_2O$ per formula unit. The rehydration of **1d** occurs in two steps with a short plateau between 20 and 30% RH, which corresponds to the phase containing about $5H_2O$. At 90% RH the original phase **1** is reproduced, which was confirmed by PXRD (Fig. S1†). Moreover, **1d** can also be obtained by keeping **1** under vacuum for about 15 hours, which was confirmed by magnetic measurements. The structure of **1d** could not be discerned from the PXRD data (Fig. S1†), however, the shift of most peaks to higher 2θ values suggests decrease in the crystallographic periods, which can be expected upon loss of crystallisation water in the non-rigid coordination polymer structure.[33,34] The thermogravimetric analysis of **1** was performed with an initial 6-hour isothermal step, during which the sample was kept under dry nitrogen flow at 25 °C (Fig. S2†). The mass loss observed in this step corroborates with the DVS measurement results. The thermal decomposition marked by a sharp decrease in mass begins at about 200 °C. The slight apparent mass loss at the beginning of the temperature rise step can be attributed to the balance drift.

In contrast to the straight chain compound **1**, the zigzag-shaped compound **2** could not be obtained in pure form from solution reaction. The synthesis of an isotypic zigzag-shaped chain based on $[W(CN)_8]^{4-}$ ions[23] was performed at 105 °C. This synthetic procedure could not be adopted, since such high temperature causes decomposition of the more fragile $[Nb(CN)_8]^{4-}$ ion. However, pure compound **2** in the powder form can be obtained in a topotactic solid-state reaction.
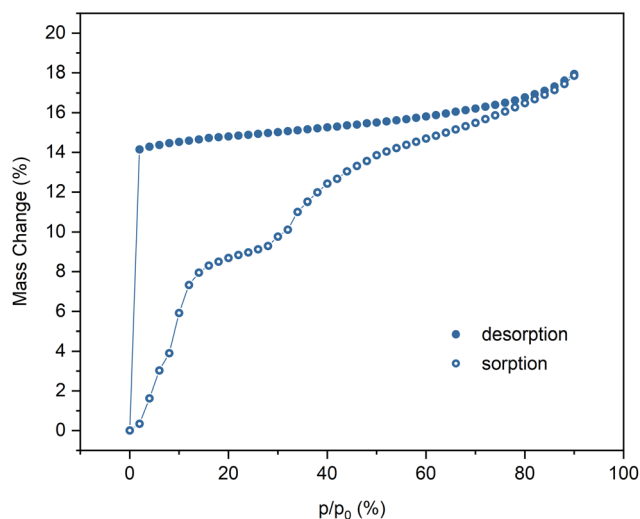

Fig. 1 Water sorption isotherm for **1** at 25 °C.

Thermal treatment of **1** or **1d** at 150 °C for one hour results in complete conversion to structure **2**, which was confirmed by PXRD (Fig. S1†). Compound **2** in both crystalline and powder form is extremely sensitive to contact with liquid water, which causes immediate decomposition. However, it remains unchanged for a few days under ambient temperature and humidity below 50% and can be kept for longer periods of time in a moisture-free atmosphere. Compound **2** can be transformed back to **1** through rehydration by exposure to 90% humidity for about 1 day. However, the transition is accompanied by partial recrystallization to the neutral Ni_2Nb polymer.[32] The thermogravimetric analysis of **2** (Fig. S3†) reflects the behaviour observed for **1** at higher temperatures, with decomposition beginning at 200 °C.

Structure description

$Li_2[Ni(cyclam)][Nb(CN)_8]\cdot7.5H_2O$ (**1**) crystallizes in the monoclinic system, space group $P2/n$ (Table 1). The asymmetric unit contains half of the $[Ni(cyclam)]^{2+}$ cation at the centre of inversion, half of the $[Nb(CN)_8]^{4-}$ anion at the 2-fold proper rotation axis as well as one Li^+ ion, and three water molecules in general positions (Fig. S4†). The niobium ion is coordinated by eight cyanide ligands with the geometry close to an ideal square antiprism (D_{4d}, CShM = 0.114, Table S1†). The nickel ion is coordinated by four N-atoms of the cyclam ligand in equatorial positions and two N-atoms of the bridging CN^- ligands in axial positions, with the geometry close to an ideal octahedron (O_h, CShM = 0.154, Table S2†). The $[Ni(cyclam)]^{2+}$ and $[Nb(CN)_8]^{4-}$ moieties are linked through CN-bridges and form 1D coordination chains along the [−101] crystallographic direction (Fig. 2). The bridging CN^- ligands are located on the opposite faces of the square antiprism forming the C1–Nb1–C1′ angle of 144.2° (Table S4†). Additionally, the CN-bridges are slightly bent with the Ni1–N1–C1 angle of 162.3°, which results in the Ni–Nb–Ni angle of 153.2° and Ni–Nb separation of 5.42 Å. The negative charge of the coordination chains, which arises from the charge disparity between the building blocks, is compensated by the presence of Li^+. The lithium

cation is surrounded by two water molecules and two N-atoms of terminal CN^- ligands, resulting in slightly distorted tetrahedral geometry (T_d, CShM = 0.611, Table S3†). The $[Li(H_2O)_2]^+$ units link the neighbouring coordination chains into two-dimensional layers in the (020) crystallographic plane (Fig. S5†). The distance between chains within one layer is 7.46 Å, while the distance between the neighbouring layers is 9.64 Å. The closest contact between the Ni and Nb centres from the adjacent chains is 7.78 Å. These values are comparable to those observed in the isotypic structure based on the $[W(CN)_8]^{4-}$ building block.[23] The layers are bound by hydrogen bonds (Table S5†) between the terminal CN ligands (N4) and the $[Li(H_2O)_2]^+$ unit (O2), as well as through the crystallization water molecule (O3) bound to the terminal cyanide (N4) and cyclam ammine group (N12). The structure contains six water molecules per formula unit, which were found from the electron density map. However, there are also well-defined solvent-accessible voids, which presumably contain the additional water found in elemental analysis and sorption measurements.[35]

$Li_2[Ni(cyclam)][Nb(CN)_8]\cdot2H_2O$ (**2**) crystallizes in the monoclinic system, space group $C2/c$ (Table 1). The asymmetric unit contains one half of the $[Nb(CN)_8]^{4-}$ anion at the 2-fold proper rotation axis, half of the $[Ni(cyclam)]^{2+}$ cation at the centre of inversion as well as one Li^+ ion and one water molecule in general positions (Fig. S6†). In contrast to **1**, the geometry of octacyanidoniobate(IV) is closer to an ideal triangular dodecahedron (D_{2d}, CShM = 0.374) rather than square antiprism (Table S1†). The octahedral environment of nickel ion is slightly more distorted than in **1** (O_h, CShM = 0.193). The CN-bridged Ni–Nb coordination chains that extend in the [001] crystallographic direction are distinctly zigzag-shaped (Fig. 3). The bridging CN^- ligands are located on the shortest edge of the triangular dodecahedron with the C1–Nb1–C1′ angle of 69.7° (Table S4†). The Ni–Nb–Ni angle within the zigzag chain is larger (86.6°), due to the marked bending of the CN-bridges, in which the Ni1–N1–C1 angle of 156.3° is smaller than in **1**. It also results in a slightly shorter Ni–Nb distance of 5.33 Å. Like
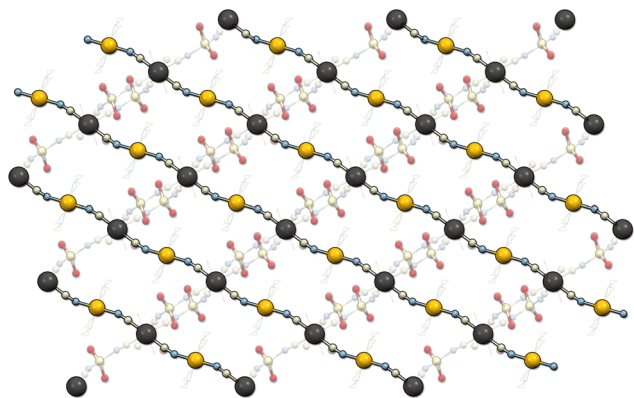

Fig. 2 Structure of **1** viewed along the [010] crystallographic direction showing the parallel straight coordination chains (Ni – orange balls, Nb – black balls) linked through the $[Li(H_2O)_2]^+$ units (shaded out).
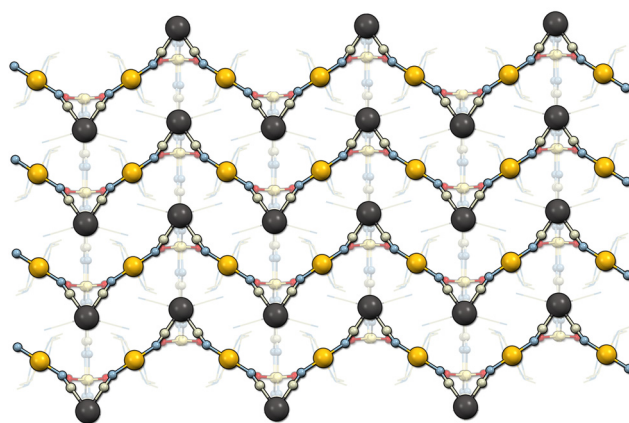

Fig. 3 Structure of **2** viewed along the [100] crystallographic direction showing the zigzag-shaped coordination chains.

in **1**, two Li^+ cations per formula unit are present in the structure to compensate the negative charge of the coordination chain, and each Li^+ centre is surrounded by two water molecules and two N atoms of terminal CN ligands. However, since compound **2** contains less crystallization water, the ratio between Li^+ and H_2O is 1:1. Therefore, two lithium cations share two water molecules and form $[Li_2(H_2O)_2]^{2+}$ units. As a result, the tetrahedral geometry of Li^+ is significantly distorted (T_d, CShM = 1.841, Table S3†). Each $[Li_2(H_2O)_2]^{2+}$ unit is bound to three Nb centres, thus linking the coordination Ni–Nb chains into a 3D network (Fig. S7†). In addition, the water molecules (O1) form hydrogen bonds to the terminal CN ligands (N4) to give connections extending in the [001] direction (Table S6†). The closest distance between the Ni and Nb centres from the neighbouring chains is 7.64 Å, which is shorter by 0.18 Å than in **1**.

Magnetic properties

All samples were carefully protected from changing the hydration level during the magnetic measurements. The crystalline sample of **1** was sealed in a glass tube under concentrated lithium chloride solution. Samples of the dehydrated **1d** phase were prepared in two ways: sample (i) was dehydrated in the DVS chamber under flow of dry nitrogen until it reached constant mass, then transferred to a glovebox and covered in nujol; sample (ii) was placed in an open glass tube, immobilized with a glass wool pad and dehydrated under vacuum for 1 day then transferred to the magnetometer and kept for additional two hours under vacuum in the magnetometer cavity. The magnetic data collected for both samples of **1d** were identical. Sample **2** was prepared by heating sample **1d** in an open glass tube at 150 °C for 1 hour. It was then transferred quickly to the magnetometer and kept for half an hour at 100 °C under vacuum in the magnetometer cavity. Detailed magnetic measurements plots are presented in Fig. S8–S10.†

The product of magnetic susceptibility and temperature (Fig. 4) in the high-temperature limit reaches 1.49, 1.46, and 1.44 cm^3 K mol^{-1} for **1**, **1d**, and **2**, respectively, which is in good agreement with the value of 1.48 cm^3 K mol^{-1} expected for one Ni^{II} ($S = 1$ and $g = 2.1$) and one Nb^{IV} ($S = 1/2$ and $g = 2.0$) per formula unit. The $\chi_M T$ signals for **1** and **2** increase with decreasing temperature reaching the maximum of 2.60 cm^3 K mol^{-1} at 8.2 K (**1**) and 2.00 cm^3 K mol^{-1} at 6.5 K (**2**). In the case of **1d**, the $\chi_M T$ curve decreases slowly below 75 K and then sharply below 6 K. The magnetization *vs.* field curves at 1.8 K (Fig. 5) show marked differences between the compounds. For **1** the initial slow linear increase is followed by an inflection point at $H_C = 15.6$ kOe and the fast increase to near saturation value of 3.10$N\beta$. In the case of the dehydrated phase **1d**, there is no discernible inflection point and the maximum magnetization value of 1.44$N\beta$ at 70 kOe is far from the expected saturation. For **2** the inflection point appears at $H_C = 8.4$ kOe and the magnetization reaches 1.93$N\beta$. The increase in $\chi_M T$ and magnetization reaching saturation indicate that ferromagnetic interactions are present within the straight chains of **1**. They arise from the orthogonality of mag-
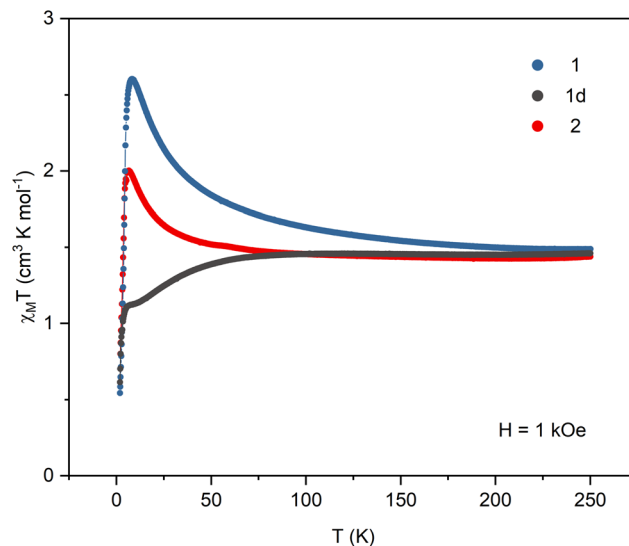

Fig. 4 The magnetic susceptibility and temperature product in the function of temperature at the applied field of 1 kOe for **1**, **1d**, and **2**.
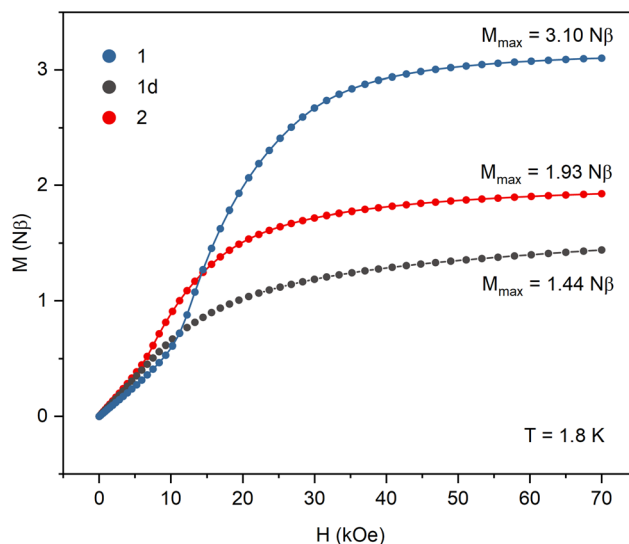

Fig. 5 The magnetization *vs.* magnetic field plot at 1.8 K for **1**, **1d**, and **2**.

netic Ni^{II} orbitals and π^* orbitals of the CN ligands and were observed in numerous Ni^{II} – cyanometallate assemblies with only slightly bent CN bridges. The antiferromagnetic interactions between the chains mediated by hydrogen bonds result in the observed field-induced metamagnetic phase transition between antiferromagnetically and ferromagnetically ordered phases at the critical field $H_C = 15.6$ kOe. This transition is also observed in the FC susceptibility measurements performed at different magnetic fields, where the maximum marking the antiferromagnetic order disappears between 15 and 20 kOe (Fig. S8†). The magnetic susceptibility data for **1** were fitted above 10 K, where the effect of inter-chain antiferro-

magnetic interactions is negligible (Fig. S8†). The chain structure was approximated by a cyclic fragment composed of 6 ions (3 Ni and 3 Nb) with isotropic interactions using the following exchange Hamiltonian: $H = -2J(S_1S_2 + S_2S_3 + S_3S_4 + S_4S_5 + S_5S_6 + S_6S_1)$. The resulting values of $J = 4.8$ (± 0.2) cm^{-1}, $g_{Ni} = 2.09$, $g_{Nb} = 2.00$ (fixed) are within the range observed for CN-bridged compounds based on Ni^{II} and octacyanometallates.[7,36,37] For the dehydrated phase **1d** the decrease in the $\chi_M T$ product with lowering temperature indicates antiferromagnetic intra-chain interactions. The fitting of the magnetic susceptibility data above 30 K (Fig. S9†) returned the values of $J = -1.94$ (± 0.08) cm^{-1} and $g_{Ni} = 2.12$. In the magnetization measurements at 1.8 K the maximum value of $1.44N\beta$ reached at 70 kOe is only slightly higher than expected for the ferrimagnetically ordered chain composed of alternating $S = 1$ and $S = 1/2$ centres. The FC susceptibility measurements at the applied field of 20 and 100 Oe show a maximum around 2.2 K, which is not present at the field of 500 Oe. This suggests that the metamagnetic phase transition between antiferromagnetically and ferrimagnetically ordered phases is present but cannot be observed in the magnetization measurements because of the low critical field. Weaker inter-chain antiferromagnetic interactions arise from the lower effective spin value but may also be affected by breaking of the hydrogen bond network upon loss of the crystallization water. Although the structure of **1d** could not be established, the negative value of the magnetic exchange constant suggests that the dehydration process causes significant bending of the CN bridges, which results in breaking the orthogonality of Ni^{II} d$_{z^2}$ and CN$^-$ $\pi^\star$ orbitals and switching from ferromagnetic to antiferromagnetic Ni^{II}–Nb^{IV} interactions within the chain. For the zigzag-shaped chain **2** the slower increase in $\chi_M T$ with decreasing temperature indicates weaker intra-chain interactions than those in the straight chain **1**. The fitting of magnetic susceptibility above 10 K (Fig. S10†) resulted in $J = 1.88$ (± 0.03) cm^{-1}, $g_{Ni} = 2.03$. The exchange constant values for **1** and **2**, together with the data available for other Ni^{II}–Nb^{IV} CN-bridged compounds[7,36] show a clear trend in the decrease of J with decreasing value of the Ni–N≡C angle (Table S7†). Similar trend was observed for the polynuclear systems based on Ni^{II} and $[M^V(CN)_8]^{3-}$ ions (M = Mo, W).[38] In contrast to **1**, for compound **2** the magnetization at 1.8 K and 70 kOe reaches only $1.93N\beta$, which is much lower than the expected saturation value. This effect can be attributed to the anisotropy of the Ni^{II} ions and their arrangement within the zigzag chain. The octahedral Ni^{II} complexes typically show magnetic anisotropy with $|D|$ ranging from 1 to 5 cm^{-1}.[39–42] In the straight chain structure of **1**, with the CN bridges along the [−101] crystallographic direction, all $[Ni(cyclam)]^{2+}$ complexes have nearly the same orientation, which ensures that their easy magnetization axes (or planes) coincide. In the zigzag chain structure of **2**, the $[Ni(cyclam)]^{2+}$ complexes have two almost perpendicular orientations, which may result in spin frustration or spin canting effects.[43,44] The inter-chain antiferromagnetic interactions between the chains result in the metamagnetic phase transition with $H_C = 8.4$ kOe, which is slightly lower than in

the case of **1**. The AC susceptibility measurements for **1**, **1d**, and **2** (Fig. S8–S10†) show no slow relaxation processes. On the basis of the temperature dependence of magnetic susceptibility measured at different fields and magnetization data, the magnetic phase diagrams for **1** and **2** were constructed, which show a rough outline of the magnetic field and temperature regions where antiferromagnetic or ferromagnetic order is present (Fig. S11†).

Conclusions

Two 1D structures: the straight Li$_2$[Ni(cyclam)][Nb(CN)$_8$]·7.5H$_2$O (**1**) chain and the zigzag-shaped Li$_2$[Ni(cyclam)][Nb(CN)$_8$]·2H$_2$O (**2**) chain were obtained by self-assembly process carried out in concentrated LiCl solution. The compounds can be interconverted by a two-step topotactic reaction resulting in ferro- to antiferromagnetic switching of the superexchange interactions through CN-bridges.

The formation of alternating bimetallic chains from [Ni(cyclam)]$^{2+}$ and [W(CN)$_8$]$^{4-}$ is hindered by charge disparity between the building blocks. This problem was overcome by the use of LiCl solution, which enabled incorporation of Li$^+$ cations into the structure to compensate the negative charge of the coordination chain. The solution reaction led to the straight chain **1**, with transient formation of the zigzag-shaped chain **2** as a by-product. The latter could be obtained in pure form by dehydration of **1** to the intermediate dihydrate phase **1d** followed by thermal treatment at 150°. The structure reorganization during the solid-state conversion from **1** to **2** is quite drastic, as the angle between the bridging cyanides changes from 144.2° to 69.6° and the [Ni(cyclam)]$^{2+}$ units are rotated. Together with high activation temperature, it indicates the possibility of temporary CN$^-$ ligand dissociation, which was found possible for related octacyanidometallates.[45–47] Our work shows the utility of the topotactic reactions, which may give access to compounds that are difficult to synthesise in solution reactions. The effects of thermally activated ligand release from the complex in solid state may be different from that in solution, where the vacant coordination site is exposed to solvent. The released ligands trapped in the crystal lattice are more likely to re-form bonds.

The structure reorganization in the topotactic reaction is accompanied by changes in magnetic properties. The intra-chain interactions change from ferro- in **1** to antiferromagnetic in **1d** and again to weaker ferromagnetic in **2**. The switching is effected by bending of the CN-bridges, which mediate magnetic superexchange, as well as the rearrangement of the relative positions of the anisotropic Ni^{II} building blocks. Switching of magnetic properties by dehydration-induced structure changes was discovered over 20 years ago[48] and later observed in several CN-bridged networks.[49–52] In most cases switching between two structures was discovered, with only a few examples of stepwise dehydration, which allowed characterisation of three phases.[10,33,34] For the presented Ni^{II}–Nb^{IV} chains we have shown that dehydration-induced structural

changes can be followed by subsequent structure reorganization activated by thermal treatment without further loss of crystallization water.

Conflicts of interest

There are no conflicts to declare.

Acknowledgements

References

1 B. Sieklucka, R. Podgajny, T. Korzeniak, B. Nowicka, D. Pinkowicz and M. Kozieł, *Eur. J. Inorg. Chem.*, 2011, 305–326.

2 S. Chorazy, J. J. Zakrzewski, M. Magott, T. Korzeniak, B. Nowicka, D. Pinkowicz, R. Podgajny and B. Sieklucka, *Chem. Soc. Rev.*, 2020, **49**, 5945–6001.

3 B. Nowicka, T. Korzeniak, O. Stefańczyk, D. Pinkowicz, S. Chorąży, R. Podgajny and B. Sieklucka, *Coord. Chem. Rev.*, 2012, **256**, 1946–1971.

4 M. Magott, B. Gaweł, M. Sarewicz, M. Reczyński, K. Ogorzały, W. Makowski and D. Pinkowicz, *Chem. Sci.*, 2021, **12**, 9176–9188.

5 B. Sieklucka and D. Pinkowicz, *Molecular Magnetic Materials*, Wiley-VCH, Weinheim, Germany, 2017.

6 J. M. Herrera, P. Franz, R. Podgajny, M. Pilkington, M. Biner, S. Decurtins, H. Stoeckli-Evans, A. Neels, R. Garde, Y. Dromzée, M. Julve, B. Sieclucka, K. Hashimoto, S. Okhoshi and M. Verdaguer, *C. R. Chim.*, 2008, **11**, 1192–1199.

7 D. Pinkowicz, R. Pełka, O. Drath, W. Nitek, M. Bałanda, A. M. Majcher, G. Poneti and B. Sieklucka, *Inorg. Chem.*, 2010, **49**, 7565–7576.

8 W. Kosaka, K. Imoto, Y. Tsunobuchi and S. Ohkoshi, *Inorg. Chem.*, 2009, **48**, 4604–4606.

9 K. Imoto, M. Takemura, H. Tokoro and S. Ohkoshi, *Eur. J. Inorg. Chem.*, 2012, 2649–2652.

10 D. Pinkowicz, R. Podgajny, B. Gaweł, W. Nitek, W. Łasocha, M. Oszajca, M. Czapla, M. Makarewicz, M. Bałanda and B. Sieklucka, *Angew. Chem., Int. Ed.*, 2011, **50**, 3973–3977.

11 D. Pinkowicz, R. Podgajny, M. Bałanda, M. Makarewicz, B. Gaweł, W. Łasocha and B. Sieklucka, *Inorg. Chem.*, 2008, **47**, 9745–9747.

12 M. Fitta, M. Bałanda, M. Mihalik, R. Pełka, D. Pinkowicz, B. Sieklucka and M. Zentkova, *J. Phys.: Condens. Matter*, 2012, **24**, 506002.

13 P. Konieczny, Ł. Michalski, R. Podgajny, S. Chorazy, R. Pełka, D. Czernia, S. Buda, J. Mlynarski, B. Sieklucka and T. Wasiutyński, *Inorg. Chem.*, 2017, **56**, 2777–2783.

14 P. Konieczny, R. Pełka, D. Czernia and R. Podgajny, *Inorg. Chem.*, 2017, **56**, 11971–11980.

15 D. Pinkowicz, R. Podgajny, W. Nitek, M. Rams, A. M. Majcher, T. Nuida, S. Ohkoshi and B. Sieklucka, *Chem. Mater.*, 2011, **23**, 21–31.

16 R. Pradhan, C. Desplanches, P. Guionneau and J. P. Sutter, *Inorg. Chem.*, 2003, **42**, 6607–6609.

17 S. L. Ma and S. Ren, *J. Inorg. Organomet. Polym.*, 2009, **19**, 382–388.

18 S. L. Ma, Y. Ma, S. Ren, S. P. Yan and D. Z. Liao, *Struct. Chem.*, 2008, **19**, 329–338.

19 N. Ozaki, R. Yamada, K. Nakabayashi and S. Ohkoshi, *Acta Crystallogr., Sect. E: Struct. Rep. Online*, 2011, **E67**, m702–m703.

20 W. Zhang, Z.-Q. Wang, O. Sato and R.-G. Xiong, *Cryst. Growth Des.*, 2009, **9**, 2050–2053.

21 H.-L. Sun, Z.-M. Wang and S. Gao, *Coord. Chem. Rev.*, 2010, **254**, 1081–1100.

22 S. Gao, *Molecular Nanomagnets and Related Phenomena*, Springer Berlin, Heidelberg, 2015.

23 M. Heczko, E. Sumińska, D. Pinkowicz and B. Nowicka, *Inorg. Chem.*, 2022, **61**, 13817–13828.

24 M. Heczko, E. Sumińska, B. Sieklucka and B. Nowicka, *CrystEngComm*, 2019, **21**, 5067–5075.

25 M. Heczko, M. Reczyński, C. Näther and B. Nowicka, *Dalton Trans.*, 2021, **50**, 7537–7544.

26 M. Reczyński, M. Heczko, M. Kozieł, S. Ohkoshi, B. Sieklucka and B. Nowicka, *Inorg. Chem.*, 2019, **58**, 15812–15823.

27 G. Handzlik, M. Magott, B. Sieklucka and D. Pinkowicz, *Eur. J. Inorg. Chem.*, 2016, 4872–4877.

28 G. M. Sheldrick, *Acta Crystallogr., Sect. A: Found. Adv.*, 2015, **A71**, 3–8.

29 C. F. Macrae, I. J. Bruno, J. A. Chisholm, P. R. Edgington, P. McCabe, E. Pidcock, L. Rodriguez-Monge, R. Taylor, J. van de Streek and P. A. Wood, *J. Appl. Crystallogr.*, 2008, **41**, 466–470.

30 D. C. M. Llunell, J. Cirera, P. Alemany and S. Alvarez, *SHAPE v. 2.1*, University of Barcelona, Spain, 2013.

31 N. F. Chilton, R. P. Anderson, L. D. Turner, A. Soncini and K. S. Murray, *J. Comput. Chem.*, 2013, **34**, 1164–1175.

32 B. Nowicka, M. Bałanda, M. Reczyński, A. M. Majcher, M. Kozieł, W. Nitek, W. Łasocha and B. Sieklucka, *Dalton Trans.*, 2013, **42**, 2616–2621.

33 B. Nowicka, M. Reczyński, M. Bałanda, M. Fitta, B. Gaweł and B. Sieklucka, *Cryst. Growth Des.*, 2016, **16**, 4736–4743.

34 R. Herchel, Z. Tuček, Z. Trávníček, D. Petridis and R. Zbořil, *Inorg. Chem.*, 2011, **50**, 9153–9163.

35 L. Glasser, *Cryst. Growth Des.*, 2019, **19**, 3397–3401.

36 T. Ohno, S. Chorazy, K. Imoto and S. Ohkoshi, *Cryst. Growth Des.*, 2016, **16**, 4119–4128.

37 D. Visinescu, C. Desplanches, I. Imaz, V. Bahers, R. Pradhan, F. A. Villamena, P. Guionneau and J.-P. Sutter, *J. Am. Chem. Soc.*, 2006, **128**, 10202–10212.

38 Y.-Q. Zhang and C.-L. Luo, *Dalton Trans.*, 2008, 4575–4584.

39 A. Wojciechowska, A. Gągor, M. Duczmal, Z. Staszak and A. Ozarowski, *Inorg. Chem.*, 2013, **52**, 4360–4371.

40 D. Schweinfurth, J. Krzystek, I. Schapiro, S. Demeshko, J. Klein, J. Telser, A. Ozarowski, C.-Y. Su, F. Meyer, M. Atanasov, F. Neese and B. Sarkar, *Inorg. Chem.*, 2013, **52**, 6880–6892.

41 R. Herchel, R. Boča, J. Krzystek, A. Ozarowski, M. Durán and J. Slageren, *J. Am. Chem. Soc.*, 2007, **129**, 10306–10307.

42 G. Novitchi, S. Jiang, S. Shova, F. Rida, I. Hlavička, M. Orlita, W. Wernsdorfer, R. Hamze, C. Martins, N. Suaud, N. Guihéry, A.-L. Barra and C. Train, *Inorg. Chem.*, 2017, **56**, 14809–14822.

43 D. Shao, S.-L. Zhang, X.-H. Zhao and X.-Y. Wang, *Chem. Commun.*, 2015, **51**, 4360–4363.

44 H. Y. Jung, H. L. Jeong, W. C. Seok, C. K. Hyoung and S. H. Chang, *Inorg. Chem.*, 2007, **46**, 1529–1531.

45 X. Qi, S. Pillet, C. Graaf, M. Magott, E. E. Bendeif, P. Guionneau, M. Rouzières, V. Marvaud, O. Stefańczyk, D. Pinkowicz and C. Mathonière, *Angew. Chem., Int. Ed.*, 2020, **59**, 3117–3121, (*Angew. Chem.*, 2020, **132**, 3141–3145).

46 K. Nakabayashi, K. Tomono, Y. Tsunobuchi, W. Kosaka and S. Ohkoshi, *Acta Crystallogr., Sect. E: Struct. Rep. Online*, 2009, **E65**, i79–i80.

47 F. J. Birk, D. Pinkowicz and K. R. Dunbar, *Angew. Chem., Int. Ed.*, 2016, **55**, 11368–11371.

48 O. Kahn, J. Larionova and J. V. Yakhmi, *Chem. – Eur. J.*, 1999, **5**, 3443–3449.

49 Y. Sato, S. Ohkoshi, K. Arai, M. Tozawa and K. Hashimoto, *J. Am. Chem. Soc.*, 2003, **125**, 14590–14595.

50 M. Ohba, K. Yoneda and S. Kitagawa, *CrystEngComm*, 2010, **12**, 159–165.

51 P. Dechambenoit and J. R. Long, *Chem. Soc. Rev.*, 2011, **40**, 3249–3265.

52 N. Yanai, W. Kaneko, K. Yoneda, M. Ohba and S. Kitagawa, *J. Am. Chem. Soc.*, 2007, **129**, 3496–3497.